Int. J. Electrochem. Sci., 17 **(2022)** Article Number: 22069, doi: 10.20964/2022.06.07

International Journal of
ELECTROCHEMICAL
SCIENCE
www.electrochemsci.org

Effect of KH-550 modified reduced graphene oxide (MrGO) content on the corrosion resistance behavior of MrGO/Epoxy Coatings in CO_2-Cl- environment

Jinling Li[1], Shusen Wang[2], Shidong Zhu[2,], Anqing Fu[3], Rui Cai[3], Naixin Lv[3], Zhigang Yang[4], Chengda Wang[4], Yan Li[1]*

[1] School of Chemistry and Chemical Engineering, Xi'an Shiyou University, Xi'an 710065, China,
[2] School of Materials Science and Engineering, Xi'an Shiyou University, Xi'an 710065, China,
[3] State Key Laboratory for Performance and Structure Safety of Petroleum Tubular Goods and Equipment Materials, CNPC Tubular Goods Research Institute, Xi'an 710077, China,
[4] Shaanxi Key Laboratory of Carbon Dioxide Sequestration and Enhanced Oil Recovery, Research Institute of Yangchang Petroleum (Group) Co. LTD, Xi'an 710065, China.
[*]E-mail: zhusdxt@126.com

Received: 5 February 2022/ *Accepted:* 25 March 2022/ *Published:* 7 May 2022

With the development of ultradeep oil and gas reservoirs, the service environment for tubing and casings is increasingly worse, resulting in higher requirements for the internal coatings, while reduced graphene oxide (rGO) is conducive to enhancing the corrosion resistance of the coatings to a certain extent. In this paper, rGO was first modified by the coupling agent KH-550 (namely, MrGO), and the physical and chemical properties (dispersibility, thermal stability, contact angle, and adhesion) of the MrGO/epoxy coatings with different MrGO contents (0.5 wt.%, 1 wt.%, 2 wt.%, 3 wt.%, and 4 wt.%) were analysed. The corrosion resistance behaviour was studied by electrochemical techniques in CO_2-Cl^- environments. The results showed that the coupling agent KH-550 was better grafted with rGO and that the diffusivity of MrGO in the MrGO/epoxy coatings was significantly improved. With an increase in the MrGO content, the physical and chemical properties of the MrGO/epoxy coatings were considerably enhanced, and the corrosion resistance first increased and then decreased; among them, the thermal stability, friction coefficient, impact performance, adhesion, and corrosion resistance of the MrGO/epoxy coatings were best when the content of MrGO was 3 wt.%. Finally, a novel corrosion resistance mechanism was proposed for the MrGO/epoxy coatings. Thus, this work provides theoretical support for the development of new heavy corrosion coatings.

Keywords: Modified rGO; Corrosion resistance; Adhesion strength; Dispersion; Electrochemical characteristics

1. INTRODUCTION

In the oil and gas industry, oil and gas fluids are often accompanied by corrosive media with

high impurities; among them, CO_2 is the most prevalent, and water is the carrier of CO_2 corrosion. As oil and gas are continuously extracted, the fluid media are acidized, and electrochemical interactions between corrosive media and oil country tubular goods (OCTGs) occur, resulting in corrosion failures from time to time [1-2]. To extend the service life of OCTGs, some technologies, including corrosion inhibitors, biocides, interior coatings, and cathodic protection, in addition to corrosion-resistant materials have been commonly used to protect OCTGs from internal corrosion [3-5]; among them, coatings are one of the easiest and most effective technologies for metal protection.

Protective coatings must have excellent bond strength, high abrasion resistance, and excellent corrosion resistance, and organic polymer coatings are the most popular coatings [6]. Since epoxy resins were discovered by Castan and Greenlee, thermosetting resins have been widely used in coating systems due to their strong mechanical properties, high adhesion, heat resistance, and corrosion resistance [7]. The curing of epoxy resins is a chemical reaction in which the epoxy groups react with the curing agent to form a highly crosslinked three-dimensional network structure. Depending on the chemical formulation of the curing agent, the curing of epoxy resins is usually in the range of 5 ℃ to 150 ℃ [8-9]. However, there are gaps between the polymer chains in the epoxy coatings, and micropores are also found due to evaporation of certain solvents during curing. The presence of these defects allows corrosive media to easily diffuse and penetrate into the metal substrate, reducing the hardness and corrosion resistance of the coatings [10]. Studies have demonstrated that the addition of organic or inorganic nanomaterials could plug micropores in coatings. Furthermore, the surface functionalization of nanoparticles (such as mica, hydrotalcite, and silica) could increase the crosslink density in the organic coatings. Thus, the corrosion resistance of the coatings was improved [11-16]. However, nanomaterials have a strong tendency to agglomerate in coatings, which leads to a nonuniform distribution of nanomaterials in the coatings [17] and reduces the physical and chemical properties of the coatings.

Graphene has promising applications in oil and gas fields due to its two-dimensional layered structure composed of carbon hexameric rings, large specific surface area, excellent chemical stability, and barrier properties against corrosive media, such as H_2O, CO_2, and Cl^-. Pourhashem et al. [18] prepared solvent-based epoxy/graphene oxide nanocomposite organic coatings that greatly improved the corrosion resistance of the metal substrate. Compared to epoxy coatings without added nanomaterials, the corrosion resistance of the epoxy composite coatings with 0.1 wt.% graphene was better due to the better dispersion of graphene, but when the graphene content reached 0.3 wt.% and 0.5 wt.%, graphene appeared to agglomerate in the coatings, and the barrier properties decreased. It was also found that graphene did not agglomerate, the epoxy resin coatings with 1.0 wt.% graphene presented the "labyrinth effect", and the corrosion current density was reduced by a factor of 10 in the polarization curve.

Currently, graphene composite anti-corrosion coatings are flourishing and are easily prepared by chemical exfoliation due to graphene oxide surfaces containing stratified structure of most oxygen-containing groups [20]. Anti-corrosion coatings modified by graphene derivatives (graphene oxide (GO) and reduced graphene oxide (rGO)) have been studied. However, there are still some problems with graphene/epoxy composite coatings, such as the large specific surface area and strong intermolecular forces between graphene and the polymer matrix and inherent incompatibilities, leading

to the disordered orientation and agglomeration of graphene nanosheets in the coatings [21-23]. Furthermore, the hydrophilic groups and conjugation-rich layer structure were present on the surface of GO and rGO [24], leading to GO or rGO not being uniformly distributed in the polymer. Therefore, the surface of GO or rGO needs to be modified with coupling agents to increase its functionality [25-26].

At present, few studies have focused on the effect of the modified rGO (MrGO) content on the corrosion behaviour of epoxy resin-based composite coatings. Therefore, MrGO with more stable properties was used as the filler, silane coupling agent KH-550 was used to modify the rGO surface, and then the physical and chemical behaviour of the MrGO/epoxy composite coatings with different MrGO contents was investigated in this paper to provide a theoretical basis for the development of new corrosion resistant coatings.

2. EXPERIMATION

2.1 Coating sample preparation

2.1.1 rGO modification

As the coupling agent has both inorganic and organic groups, this unique structure can be chemically bonded with the functional groups on inorganic material surfaces as well as with those on organic material surfaces. The two "incompatible" materials were close together, and the bonding and compatibility between the filler and the coatings were improved. Therefore, the coupling agent KH550 was used to modify reduced graphene oxide (MrGO).

2.1.2 Coating preparation

Epoxy resin (EP, E-08) was used as the base material, polyetheramine (D230) was used as the curing agent, and MrGO was used as the filler. Different MrGO contents (0.5 wt.%, 1 wt.%, 2 wt.%, 3 wt.%, and 4 wt.%) were added to E-08, and the composite coatings were prepared by the ultrasonic method [27]. The matrix was N80 carbon steel, and the coating thickness was 200±10 μm.

2.2 Physical and chemical performance analysis

2.2.1 Zeta potential

The zeta potential, as a valid parameter for colloids, can qualitatively characterize the stability performance of the MrGO/epoxy coatings. The coatings without a curing agent were diluted 50 times with cyclohexanone and sonicated for 30 min. A zeta potentiometer (model Zeta PALS 190 Plus) was used for zeta potential measurements.

2.2.2 Raman spectroscopy test

As it is difficult to observe the distribution of MrGO in the coatings, Raman mapping analysis was performed on the MrGO/epoxy coating surface. A complete Raman spectrum was obtained for

each point within a limited area of the specimen and then analysed by specialised software to obtain an accurate Raman image, which visually represented the distribution of MrGO in the coatings. The laser beam was focused using a 50× objective to perform the test, and the spectrum was calibrated using the 520 cm^{-1} peak of the silicon wafer. The static scan centre peak was 3000 cm^{-1}, the scan step of the streamline was 1.2 μm, the exposure time was 5 s, the cumulative number was 1, and the laser power was 100%. The scan step of the map image streamline HR was 0.5 μm, the exposure time was 0.1 s, the number of accumulations was 1, and the laser power was 50%. The scanning area was 100×80 μm^2, and the system controlled the laser to collect Raman spectra at each point in sequence from left to right and from top to bottom according to the parameter settings.

2.2.3 Thermal stability

The thermal stability of the MrGO/epoxy coatings was determined by thermogravimetric analysis (STA7000): the micro weight of the sample was weighed by an electronic balance, and the thermal stability was analysed by a thermogravimetric analyser. The experiments were carried out under a N_2 atmosphere with a N_2 flow rate of 20 ml/min, and the furnace temperature was raised from room temperature to 800 °C at a rate of 20 °C/min.

2.2.4 Contact angle

The water contact angle of the MrGO/epoxy coatings was tested using a JC2000D1 contact angle tester, a 0.725 mm needle and a droplet volume of 10 μL. The same experiment was repeated three times, and the water contact angle of the MrGO/epoxy coatings was taken as the average of the droplets' left and right contact angles.

2.2.5 Adhesion

The test was carried out in accordance with GB. T5210-2006: “Paint and varnish—pull-out adhesion test”. Six tests were conducted on each group of samples (100 mm × 50 mm × 3 mm), and the maximum test value was taken as the adhesion between the coatings and metal (unit: MPa).

2.3 Corrosion resistance

2.3.1 Electrochemical test

Electrochemical tests were carried out using a Princeton electrochemical workstation (P4000). The electrochemical impedance and polarisation curves of the MrGO/epoxy coatings were tested using a three-electrode system with a platinum electrode as the auxiliary electrode, a saturated glycerine electrode (SCE) as the reference electrode, and N80 steel coated with MrGO/epoxy as the working electrode, which was immersed in 10 wt.% NaCl solution at 80 °C. The immersion times were 60 h, 120 h, and 240 h, N_2 gas was introduced into the solution for 2 h before the deoxygenation test, and CO_2 in the solution was saturated during the test. The frequency range for impedance testing was 10^5 Hz ~ 10^{-2} Hz. The Tafel polarization curve was created with a potential scan interval of -0.5 V to 0.5 V

and a scan rate of 0.5 mV/s.

2.3.2 Simulated immersion test

Considering the actual service conditions of the MrGO/epoxy coatings, an autoclave was used to simulate the high-temperature and high-pressure environment. The experimental temperature was set at 120 ℃, the total pressure was 15 MPa (including 5 MPa CO_2 partial pressure), the experimental times were 120 h and 240 h, and the corrosion medium was a 10 wt.% NaCl solution.

3. RESULTS AND DISCUSSION

3.1 rGO modification

Figure 1 shows the IR spectra of rGO before and after modification. New absorption peaks were obviously present at 2924 cm^{-1} and 2851 cm^{-1} after the surface modification of rGO by KH550, which were the stretching vibration peaks of the methyl group and methylene group of KH550, respectively, indicating that KH550 was successfully grafted to rGO.

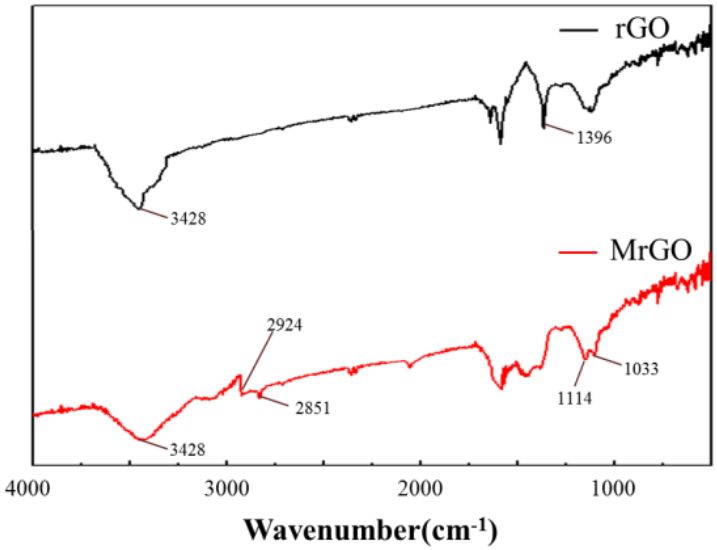

Figure 1. Infrared absorption spectra of rGO before and after modification.

3.2 rGO dispersion

3.2.1 Dispersion observation

The MrGO powder and rGO powder were added to epoxy resin (E-08) and diluted 10 times with cyclohexanone. The solution was dispersed by ultrasound for 1 h and then left to stand at room temperature. The morphology is shown in Figure 2. rGO completely sunk to the bottom of the solution after 12 h. Significant delamination of MrGO was not found, indicating that MrGO maintained good dispersion over a long period and sank very slowly. Therefore, the dispersion of rGO was greatly

improved by the grafting of silane coupling agents.

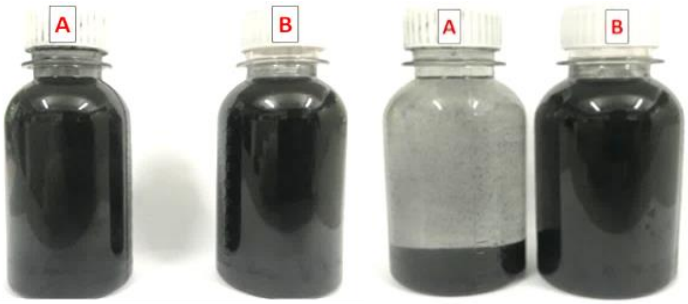

(a) (b)

Figure 2. Dispersion stability of rGO (A) and MrGO (B) in epoxy resins under different time conditions: (a) resting 0 h and (b) resting 12 h.

3.2.2 Zeta potential

Figure 3 shows the zeta potential of the MrGO/epoxy coatings with different MrGO contents. As shown in Figure 3, the peak zeta potential of the MrGO/epoxy coatings gradually decreased with increasing MrGO content, indicating that the MrGO content affected its dispersibility in the epoxy coatings.

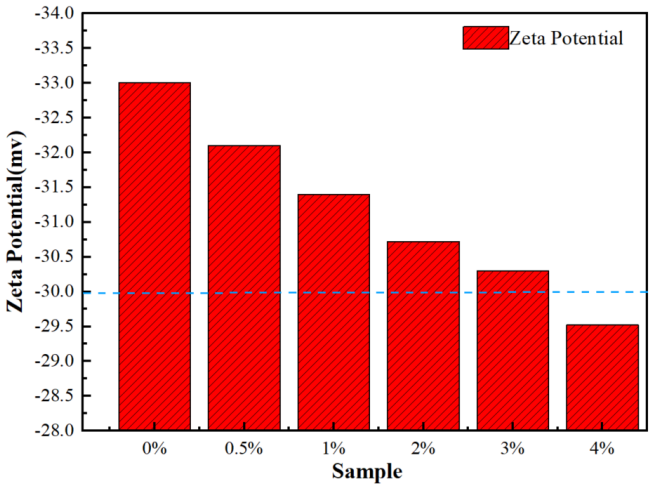

Figure 3. Zeta potential of the epoxy coatings with different MrGO contents.

According to DLVO theory [27], the zeta potential threshold value of MrGO/epoxy coatings was ± 30 mV, and a value greater than +30 mV or less than -30 mV indicated that graphene had sufficient mutual repulsion in the coatings to ensure good dispersion stability. A carboxyl group (-COOH) carried by rGO would itself be negatively charged due to its disassociation from H^+ in a weak alkali environment, and charge repulsion between colloidal particles prevented collision coalescence. Furthermore, van der Waals forces existed between the solvate ions, and the stability of the sol under

certain conditions depended on the repulsion between colloidal particles and the neutralization of van der Waals forces. When the MrGO content was 4 wt.%, the peak of the zeta potential was higher than the threshold value (-30 mV), indicating that the accumulation of MrGO occurred at this time, the amount of hydroxyl and ionized H^+ in carboxyl groups decreased, and the zeta potential increased. Therefore, 3 wt.% MrGO would maintain good dispersion in epoxy resin coatings, leading to an increase in the corrosion resistance of the MrGO/epoxy coatings.

3.2.3 Raman spectroscopy test

The Raman spectra of the MrGO/epoxy coatings with different MrGO contents are shown in Figure 4. It is obvious that the composite coatings have a broad characteristic peak near 1589 cm^{-1}, which was the G peak (main characteristic peak) of C derived from the E2g phonon first-order scattering of the in-plane vibration of the sp^2 C atom, which could effectively characterize the number of the MrGO/epoxy coatings. The D peak, formed from the vibration of the sp3 carbon atoms, appeared near 1334 cm^{-1} and reflected the structural defects in the carbon plane of the MrGO and the disordered structure of the sp^2 region due to the reduction of the planar aromatic region during oxidation [30]. The MrGO defect peak (D peak) appeared within the 200 μm Raman line sweep, indicating that MrGO had excellent diffusivity in the epoxy resin. Therefore, the D and G peaks of the Raman spectra were enhanced with increasing MrGO content, indicating that the functionalization process changed the lattice structure of the MrGO flakes [31]. However, the intensity of the D peak was stronger than that of the G peak, so the D peak was used as the scanning base peak in the Raman mapping test to characterize the dispersion of MrGO in the MrGO/epoxy coatings with increasing MrGO content.

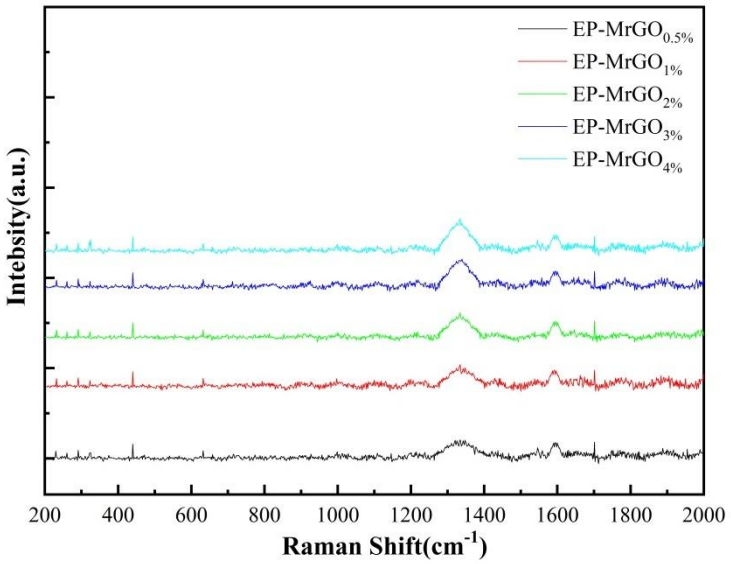

Figure 4. Raman spectra of the samples coated with different MrGO contents.

Figures 5(a1)~(f1) show the optical images of the MrGO/epoxy coatings, and Figures

5(a2)~(f2) show the component distribution maps of the Raman spectra of the MrGO/epoxy coatings after component analysis of the scanned data in the mapping region. The distribution of the two phases and a detailed characterization of the interface areas between the two phases (the interlinked phases of MrGO and epoxy molecular chains and the third phase) were accurately presented, in which the brighter areas in the Raman image were MrGO, and the darker areas were epoxy resin. It can be seen that two phases of MrGO and epoxy resin were distributed in a "sea-island" structure, in which the "island" was the dispersed MrGO phase and the "sea" was the continuous epoxy resin phase. With the increase in the MrGO content in the MrGO/epoxy coatings, the two phases gradually separated from each other in an entangled state, and the scope of the "island" gradually increased. Especially when the MrGO content reached 4 wt.%, the image was almost entirely covered by the red "island" area, indicating that rGO in the MrGO/epoxy coatings appeared agglomerated and overlapped, and the two phases became narrower, as shown in Figure 5(f2).

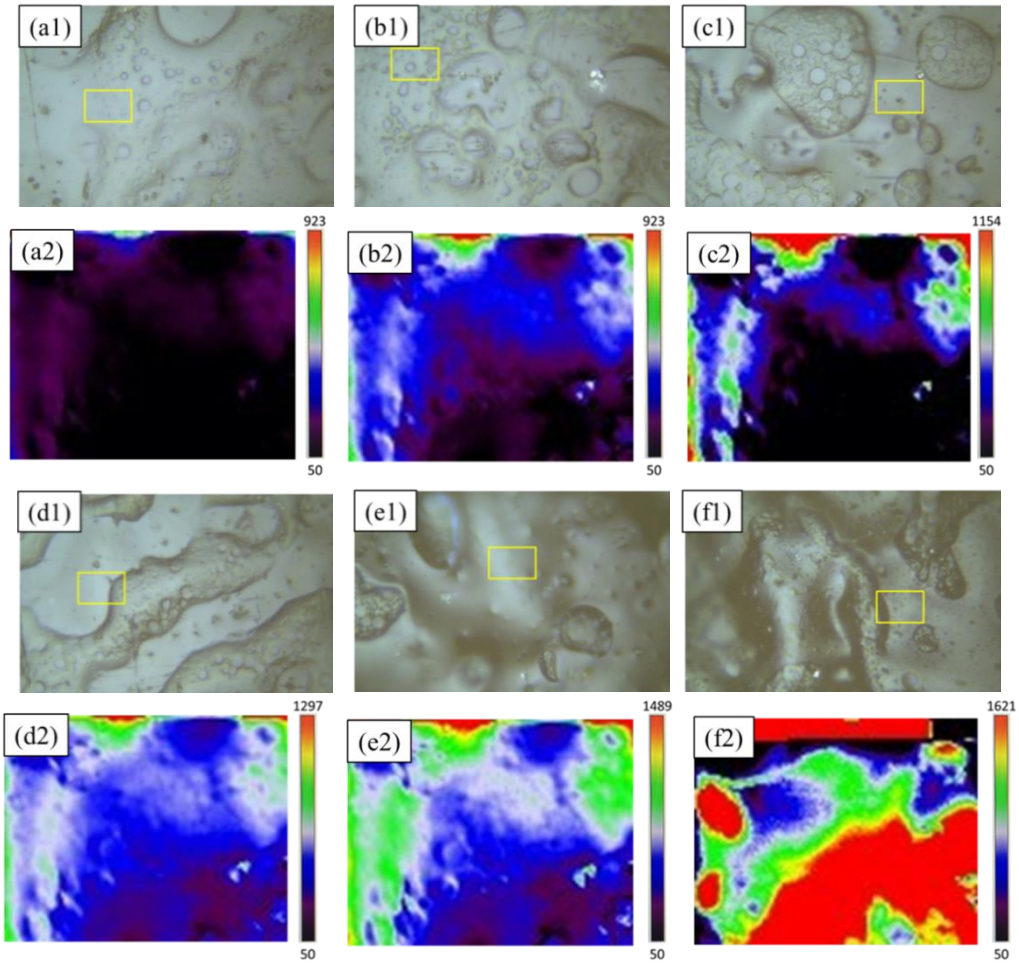

Figure 5. Optical images of the MrGO/epoxy coatings (a1, b1, c1, d1, e1, f1) and Raman imaging (a2, b2, c2, d2, e2, f2): (a) 0 wt.%, (b) 0.5 wt.%, (c) 1 wt.%, (d) 2 wt.%, (e) 3 wt.%, and (f) 4 wt.%.

3.3 Thermal stability

Figure 6 shows the thermal weight loss curve of the MrGO/epoxy coatings. It is clear that the quality did not change below 350 ℃. The weight loss occurred mainly between 350 ℃ and 650 ℃ due to the degradation of macromolecular chains of the MrGO/epoxy coatings and solid interfacial interactions [32]. The good thermal conductivity of MrGO was maximized due to the minor oxidation of functional groups, which enhanced the thermal stability of the MrGO/epoxy coatings. From Table 1, it can be seen that when the weight loss rate of the coatings was 5%, 10% and 45%, the corresponding temperature of the epoxy coatings was less than that of the MrGO/epoxy coatings, indicating that the addition of MrGO increased the thermal decomposition temperature and the thermal stability of the coatings. Furthermore, the decomposition temperature first increased and then decreased with increasing MrGO content, and the maximum was observed when the MrGO content was 3 wt.%. When the MrGO content reached 4 wt.%, the decomposition temperature of the MrGO epoxy coating with a 45% weight loss rate dropped from 579 ℃ to 544 ℃, indicating that MrGO agglomerated in the coatings, and the thermal stability of the coatings was reduced. There were two main reasons: (1) as the MrGO content in the MrGO/epoxy coatings increased, the elemental carbon content increased, which helped to enhance the thermal stability of the MrGO/epoxy coatings [33]; and (2) MrGO might hinder the epoxy resin from curing. Wei et al. [7] also argued that the functional groups on the surface of MrGO reacted with the curing agent or epoxy resin or that the large surface area of MrGO covered the reactive sites in epoxy resin. Therefore, the higher MrGO content in the MrGO/epoxy coatings decreased its dispersion, weakened the interaction between the MrGO, which appeared agglomerated, and the epoxy resin, destroyed the cross-linked epoxy resin network, and then decreased the thermal stability of the composite coatings. Therefore, it is necessary to keep the MrGO content at 3 wt.% to increase the thermal stability of the MrGO/epoxy coatings.

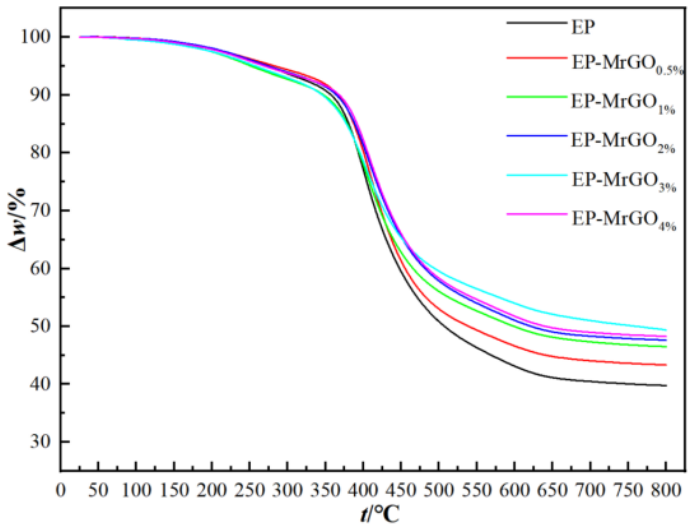

Figure 6. Thermal weight loss curves for the MrGO/epoxy coatings.

Table 1. Analysis of the thermal weight loss data for MrGO/epoxy coatings.

Weight loss rate	EP/°C	EP-MrGO$_{0.5\%}$/°C	EP-MrGO$_{1\%}$/°C	EP-MrGO$_{2\%}$/°C	EP-MrGO$_{3\%}$/°C	EP-MrGO$_{4\%}$/°C
5%	251	257	265	274	282	269
20%	373	394	403	415	427	416
45%	471	483	513	535	579	544

3.4 Hydrophobicity

The static water contact angle can determine hydrophilic and hydrophobic surfaces. Once the angle between the water droplet and the surface of the coatings has stabilized, the hydrophobic characteristic of the surface will be determined. The greater the water contact angle, the lower the surface tension and the more hydrophobic the surface material [34]. Figure 7 shows the change in contact angle of the MrGO/epoxy coatings with different MrGO contents before and after immersion in 10 wt.% NaCl solution. The contact angle of all coatings decreased after immersion for 240 h; for example, the water contact angle of epoxy coatings changed from 69.4° ± 1° to 64.5° ± 1° after the immersion experiment. The water contact angle of the MrGO/epoxy coatings showed an increasing and then decreasing trend with an increase in rGO content, and the maximum value (89.2 ± 1°) was observed when the MrGO content was 3 wt.%. The resistance to the penetration of corrosive media increases as the contact angle of the coatings increases. Therefore, 3 wt.% MrGO allowed the coatings to have the best surface roughness, leading to excellent hydrophobicity, and the water-repellent surface reduced the contact area between the coatings and the corrosive medium, reducing the content of the corrosive medium diffusing to the inside of the coatings and then slowing down the corrosion of the metal substrate.

The water contact angles of the epoxy coatings and MrGO/epoxy coatings after immersion were different, and the reasons might be the increase in hydrophilic corrosion products on the surface of the MrGO/epoxy coatings with increasing immersion time, which destroyed the density and mechanical strength of the MrGO/epoxy coatings, making the hydrophilicity of the MrGO/epoxy coatings gradually increase. On the other hand, the change in the chemical composition made the surface of the MrGO/epoxy coatings change from hydrophobic to hydrophilic. The contact angle of the MrGO/epoxy coatings with 3 wt.% rGO was larger after immersion for 240 h and possessed a certain degree of hydrophobicity but still maintained good impermeability to corrosive media. Therefore, MrGO was more effective in enhancing the corrosion resistance of the coatings by increasing the hydrophobicity of the coatings.

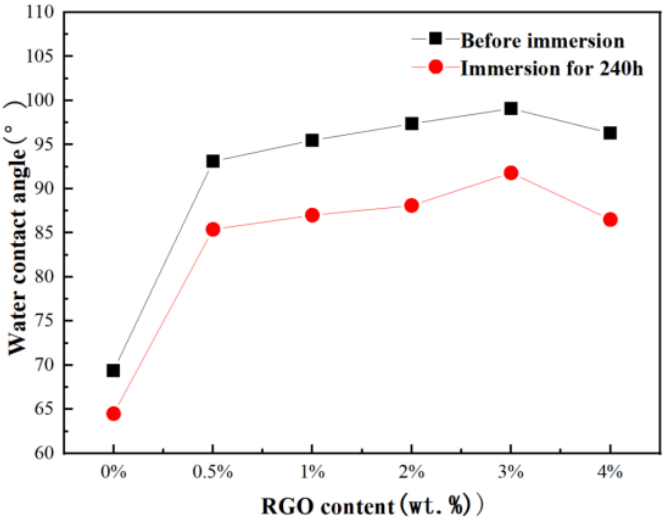

Figure 7. Water contact angle curves for the MrGO/epoxy coatings.

3.5 Coating adhesion

Table 2 shows the adhesion of the MrGO/epoxy coatings before and after immersion, and Figure 8 shows the SEM cross-sectional microscopic morphology of the MrGO/epoxy coatings with different MrGO contents. The adhesion of the MrGO/epoxy coatings exhibited a slight increase with an increasing amount of MrGO before immersion. The smaller amount of MrGO would fill the pores in the epoxy coatings, and as the MrGO content increased, the number of pores in the coatings decreased, resulting in a slight increase in adhesion in the dry film state. When the MrGO content was too high, MrGO began to agglomerate, the number of defects inside the coatings increased, and the adhesion decreased.

During the soaking phase of the coatings, the adhesion of the epoxy coatings was reduced exponentially due to a large number of pores in the epoxy coatings, while the adhesion of the epoxy coatings was significantly enhanced by the addition of MrGO. The corrosive medium easily entered the coatings through the pores and diffused to the interface between the coatings and metal substrate, which eroded the metal substrate and affected the adhesion between the coatings and metal substrate, decreasing the adhesion of the coatings [31]. On the one hand, the addition of MrGO increased the hydrophobicity of the coatings, reduced the contact area between the corrosive medium and the coatings, and increased the corrosion resistance of the coatings; on the other hand, MrGO filled the internal pores of the coatings, enhanced the barrier effect of the coatings to the corrosion medium, and extended the diffusion path of the corrosive medium. Therefore, the MrGO/epoxy coatings with 3 wt.% MrGO had good adhesion, and the corrosion resistance to the corrosive medium was enhanced.

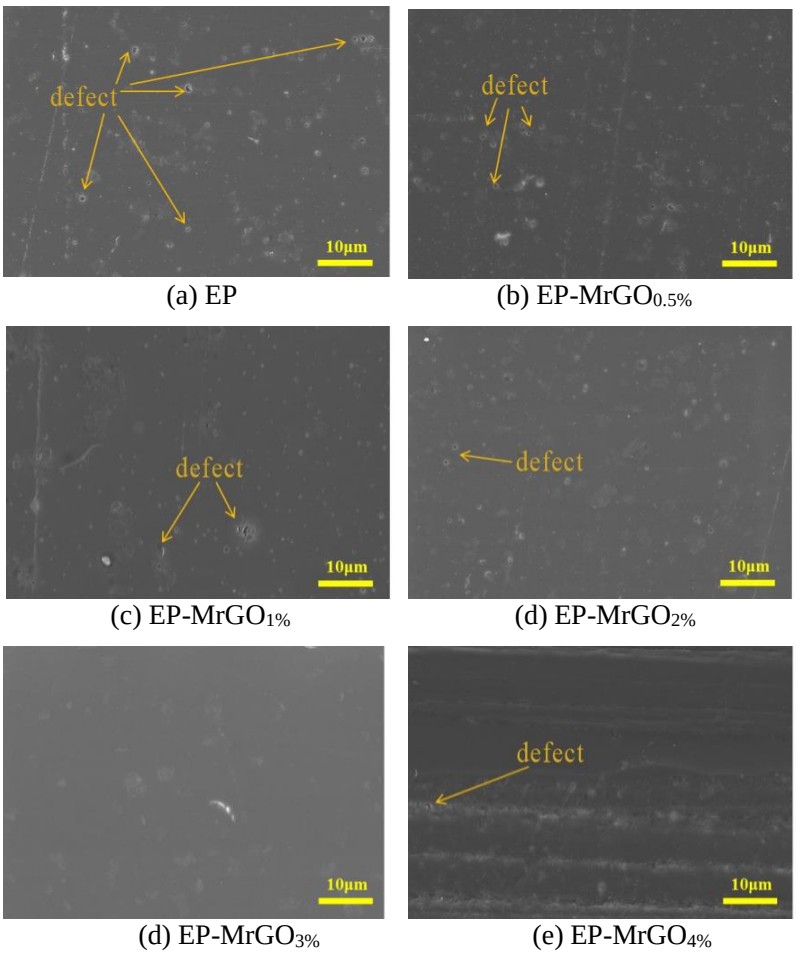

(a) EP (b) EP-MrGO$_{0.5\%}$

(c) EP-MrGO$_{1\%}$ (d) EP-MrGO$_{2\%}$

(d) EP-MrGO$_{3\%}$ (e) EP-MrGO$_{4\%}$

Figure 8. SEM cross-sectional microscopic morphology of the MrGO/epoxy coatings with different MrGO contents.

Table 2. Adhesion test data before and after immersion of the MrGO/epoxy coatings.

MrGO Content/wt.%	Adhesion/MPa		
	Before immersion	After 60 h immersion	After 120 h immersion
0	11.32	7.23	5.44
0.5	11.40	7.84	6.03
1	11.57	8.25	6.75
2	11.65	8.78	7.31
3	11.78	9.37	7.94
4	11.29	8.64	7.35

3.6 Electrochemical characteristics

3.6.1. Nyquist impedance curve

The corrosion resistance of the MrGO/epoxy coatings can be characterized using an

electrochemical Nyquist impedance curve [35]. Figure 9 shows the corrosion resistance of the MrGO/epoxy coatings after different immersion times. As shown in Figure 9(a), after soaking for 60 h, the capacitive resistance arc of the coatings showed an upwards and then downwards trend as the MrGO content increased. The impedance arc reached the maximum when the MrGO content reached 3 wt.%, which was probably due to the hydrophobicity of MrGO and the tight layer spacing of MrGO. Nair et al. argued that the electrolyte flux was effectively resisted [36]. When the MrGO content reached 4 wt.%, the impedance arc started to decrease, which was due to the excessive addition of MrGO, the agglomeration of MrGO increased the defects in the coatings, and the corrosion resistance of the coatings was reduced [34].

The MrGO/epoxy coating impedance map was fitted using the equivalent circuit shown in Figure 10(a), and the fitted data are shown in Table 3, where R_s represents the solution resistance, C_c and R_c represent the MrGO/epoxy coating capacitance and MrGO/epoxy coating resistance, respectively, C_{dl} and R_{ct} are the double-layer capacitance and charge transfer resistance, respectively, and W is the Warburg resistance. Both R_{ct} and R_c increased and then decreased with increasing MrGO content. When the MrGO content was 3 wt.%, R_{ct} (1.953×10^{9} Ω·cm^2) and R_c (3.421×10^{8} Ω·cm^2) both reached their maximum values, in which R_{ct} directly reflects the corrosion rate at the interface between the MrGO/epoxy coatings and the metal substrate, indicating that corrosion resistance was best at this time, and C_c (1.151×10^{-10} F/cm^2) reached the minimum value [37].

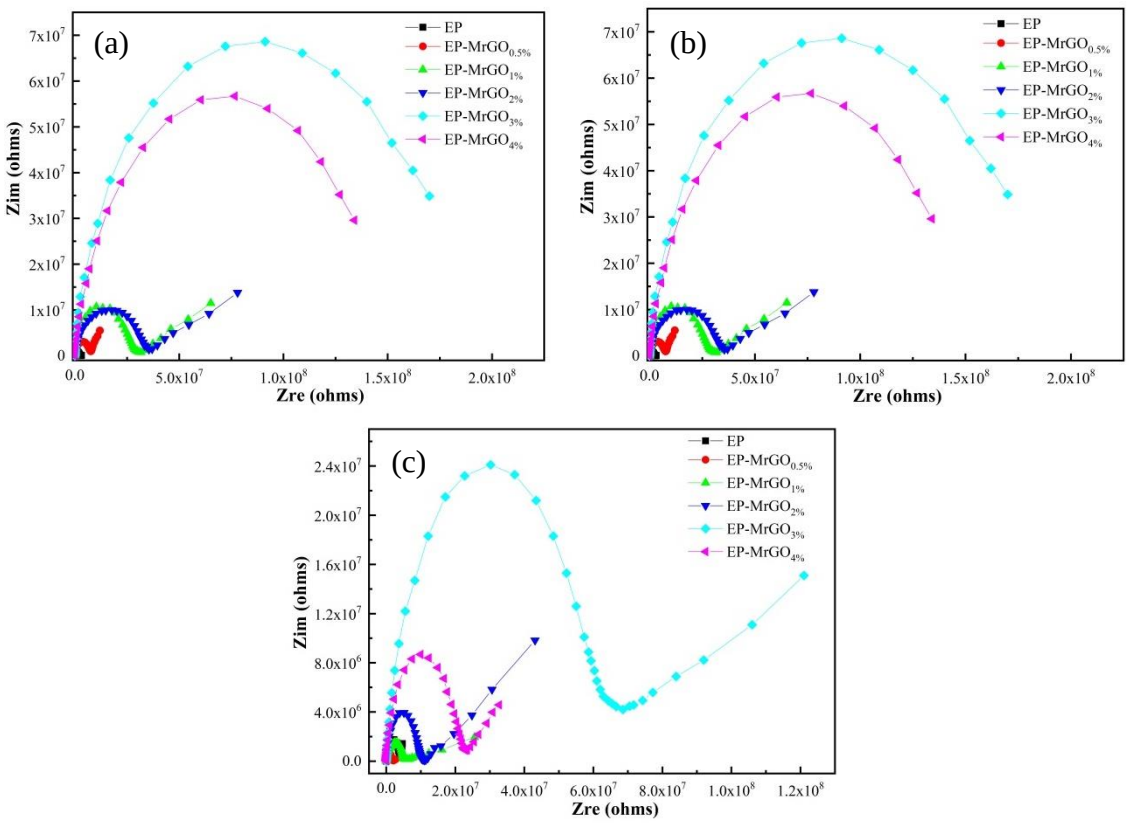

Figure 9. Nyquist plots of MrGO/epoxy coatings immersed for different times: (a) soaking for 60 h, (b) soaking for 120 h, and (c) soaking for 240 h.

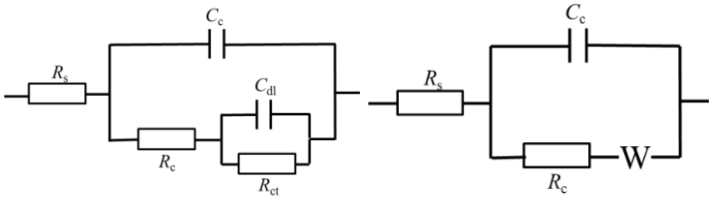

(a) (b)

Figure 10. Equivalent circuit diagram of Fig. 9.

Table 3. Data fitting of impedance equivalent circuit diagrams after different times of the MrGO/epoxy coatings after immersion for different times.

Soaking Time	Specimen	R_s/Ω·cm^2	C_c/F/cm^2	R_c/Ω·cm^2	C_{dl}/F/cm^2	R_{ct}/Ω·cm^2	W/Ω·cm^2
60 h	EP	1.585×10^{-3}	4.817×10^{-10}	6.956×10^{6}	6.244×10^{-7}	3.581×10^{7}	/
	EP-rGO0.5%	1.699×10^{-3}	3.041×10^{-10}	6.455×10^{7}	6.851×10^{-9}	1.403×10^{8}	/
	EP-rGO1%	1.320×10^{-3}	2.095×10^{-10}	1.664×10^{8}	8.883×10^{-9}	5.606×10^{8}	/
	EP-rGO2%	3.845×10^{-3}	1.451×10^{-10}	2.183×10^{8}	1.082×10^{-10}	1.161×10^{9}	/
	EP-rGO3%	1.77×10^{-3}	1.151×10^{-10}	3.421×10^{8}	1.481×10^{-10}	1.953×10^{9}	/
	EP-rGO4%	9.049×10^{-3}	2.071×10^{-10}	3.125×10^{8}	1.101×10^{-10}	7.707×10^{8}	/
120 h	EP	1.699×10^{-3}	8.707×10^{-9}	9.455×10^{5}	/	/	1.366×10^{-7}
	EP-rGO0.5%	6.379×10^{-2}	5.305×10^{-10}	2.278×10^{6}	/	/	8.354×10^{-7}
	EP-rGO1%	3.991×10^{-2}	3.912×10^{-10}	2.694×10^{7}	/	/	7.174×10^{-8}
	EP-rGO2%	1.636×10^{-1}	3.724×10^{-10}	6.721×10^{7}	/	/	6.006×10^{-8}
	EP-rGO3%	3.092×10^{-2}	2.206×10^{-10}	1.833×10^{8}	1.003×10^{-8}	1.124×10^{9}	/
	EP-rGO4%	6.168×10^{-1}	2.802×10^{-10}	1.469×10^{8}	5.14×10^{-9}	2.694×10^{8}	/
240 h	EP	3.613×10^{-2}	1.161×10^{-8}	3.715×10^{5}	/	/	1.216×10^{-6}
	EP-rGO0.5%	3.974×10^{-3}	3.418×10^{-9}	1.823×10^{6}	/	/	2.166×10^{-6}
	EP-rGO1%	1.142×10^{-2}	9.181×10^{-10}	4.465×10^{6}	/	/	3.222×10^{-7}
	EP-rGO2%	2.987×10^{-3}	5.116×10^{-10}	9.083×10^{6}	/	/	1.887×10^{-7}
	EP-rGO3%	1.102×10^{-3}	3.870×10^{-10}	4.731×10^{7}	/	/	9.247×10^{-9}
	EP-rGO4%	3.094×10^{-3}	5.124×10^{-10}	1.019×10^{7}	/	/	9.496×10^{-8}

After soaking for 120 h, the impedance spectra of EP, EP-$MrGO_{0.5\%}$, EP-$MrGO_{1\%}$, and EP-$MrGO_{2\%}$ all presented a time constant and Warburg impedance characteristics. In addition, EP-$MrGO_{3\%}$ and EP-$MrGO_{4\%}$ still showed a single capacitance resistance arc, and the capacitive arc radius first significantly increased and then decreased with increasing MrGO content, indicating that water and corrosive media had penetrated the MrGO/epoxy coatings and reached the metal surface. Finally, the impedance modulus of the MrGO/epoxy coatings decreased compared to that after soaking for 60 h. After soaking for 240 h, the MrGO/epoxy coatings all showed a time constant and Warburg impedance characteristics, fitted by the circuit diagram shown in Fig. 10(b), and the matched results are shown in Table 3. The results showed that the corrosive medium spread to the interface between the MrGO/epoxy coatings and metal substrate, and the corrosion of the metal substrate took place. However, an optimum MrGO addition of 3 wt.% greatly improved the corrosion resistance of the coatings.

Bigdeli et al. [38] argued that when R_c exceeded 1.0×10^{8} Ω·cm^2, organic coatings have

excellent corrosion resistance; when R_c is between 1.0×10^6 and 1.0×10^8 $\Omega\cdot cm^2$, organic coatings have good corrosion resistance; and when R_c is less than 1.0×10^6 $\Omega\cdot cm^2$, organic coatings have the worst corrosion resistance. Therefore, epoxy resin coatings had nearly failed after immersion for 120 h, and the corrosive medium easily penetrated EP, EP-$MrGO_{0.5\%}$, EP-$MrGO_{1\%}$ and EP-$MrGO_{2\%}$ and reached the interface between the MrGO/epoxy coatings and metal substrate within a short time. While for EP-$MrGO_{3\%}$, MrGO was added in sufficient quantity and was well dispersed in the coatings, the corrosive medium could be better prevented from penetrating the MrGO/epoxy coatings, and then the corrosion resistance of the MrGO/epoxy coatings with 3 wt% MrGO (EP-$rGO_{3\%}$) was excellent. However, the amount of MrGO in EP-$rGO_{4\%}$ was too high, and agglomeration occurred due to the uneven dispersion of MrGO in the coatings, which increased the number of defects in the MrGO/epoxy coatings and led to a reduction in the corrosion resistance of the MrGO/epoxy coatings.

3.6.2. Polarization curve

Conductive polymers are widely used in the field of anticorrosion coatings because they can passivate metal surfaces. In a corrosive environment, the coatings with conductive polymers tend to form a "microcurrent" in the corrosive system under the action of the conductive polymer, which electrochemically passivates the metal to reduce the likelihood of corrosion [34]. Graphene has a conductivity of 15000 $cm^2/(V\cdot s)$, which is similar to that of a conductive polymer.

Fig. 11 shows the polarization curves of the MrGO/epoxy coatings at different immersion times, and Table 4 shows the corresponding fitted data. It is obvious that the corrosion potential (E_{corr}) of the coatings gradually shifted positively, the corrosion current density (i_{corr}) gradually decreased, and the polarization resistance (R_P) gradually increased with increasing MrGO content in the range of 0 wt.% to 3 wt.% for the same soaking time, indicating that MrGO played a barrier role in the enhancement of the corrosion resistance of the coatings [39-42]. The lowest i_{corr}, highest E_{corr}, and largest R_P were observed when the MrGO content in the coatings was 3 wt.% for different immersion times. When the MrGO content was increased up to 4 wt.%, the E_{corr} of the coatings decreased, i_{corr} increased, and R_P decreased. Therefore, the corrosion resistance of the MrGO/epoxy coatings was better than that of the epoxy coatings, and among them, the best corrosion resistance was achieved when the coatings were made of 3 wt.% MrGO.

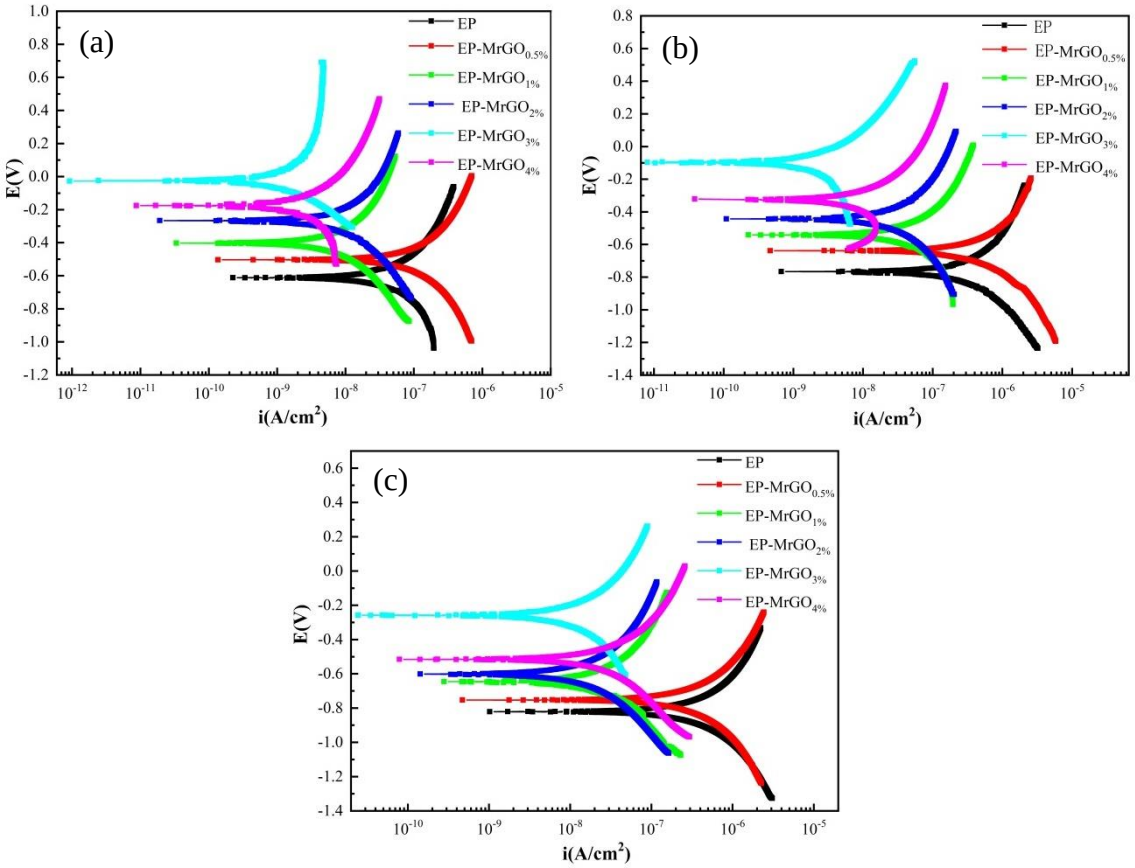

Figure 11. Tafel curves of the MrGO/epoxy coatings immersed for different times: (a) soaking for 60 h, (b) soaking for 120 h, and (c) soaking for 240 h.

Table 4. Polarization curve fitting data for MrGO/epoxy coatings after different immersion times.

Soaking Time	Specimen	E_{corr}/V	i_{corr}/A/cm^2	R_P/Ω·cm^2
60 h	EP	-0.611	2.25×10^{-10}	9.04×10^{6}
	EP-rGO$_{0.5\%}$	-0.503	1.36×10^{-10}	1.24×10^{7}
	EP-rGO$_{1\%}$	-0.402	3.35×10^{-11}	4.44×10^{7}
	EP-rGO$_{2\%}$	-0.266	1.92×10^{-11}	6.03×10^{7}
	EP-rGO$_{3\%}$	-0.027	9.22×10^{-13}	1.75×10^{8}
	EP-rGO$_{4\%}$	-0.175	8.69×10^{-12}	5.46×10^{7}
120 h	EP	-0.766	6.71×10^{-10}	2.12×10^{6}
	EP-rGO$_{0.5\%}$	-0.639	4.64×10^{-10}	6.63×10^{6}
	EP-rGO$_{1\%}$	-0.541	2.15×10^{-10}	2.18×10^{7}
	EP-rGO$_{2\%}$	-0.443	1.09×10^{-10}	6.91×10^{7}
	EP-rGO$_{3\%}$	-0.097	8.03×10^{-12}	8.97×10^{7}
	EP-rGO$_{4\%}$	-0.322	3.83×10^{-11}	7.07×10^{7}
240 h	EP	-0.822	1.02×10^{-9}	8.96×10^{5}
	EP-rGO$_{0.5\%}$	-0.754	4.71×10^{-10}	3.63×10^{6}
	EP-rGO$_{1\%}$	-0.645	2.79×10^{-10}	8.18×10^{6}
	EP-rGO$_{2\%}$	-0.602	1.42×10^{-10}	2.91×10^{7}
	EP-rGO$_{3\%}$	-0.258	2.43×10^{-11}	4.97×10^{7}
	EP-rGO$_{4\%}$	-0.515	7.88×10^{-11}	2.07×10^{7}

3.7 Surface characteristics

Fig. 12 illustrates the surface properties of the MrGO/epoxy coatings under high-temperature and high-pressure conditions. As seen in Figure 12(a), before the immersion experiment, the surface of the MrGO/epoxy coatings was flat, free of defects, bright black, and full gloss. After immersion for 120 h, the surface of the layer was blistered, indicating the proximity of the corrosive medium or the formation of diffusion holes in contact with the substrate. With the increase in the MrGO/epoxy content, the blister defects on the coating surface slightly improved, and the blister characteristics changed from dense and large volumes to sparse and small volumes, which indicated that the addition of the laminar structure of MrGO prolonged the time of corrosion media diffusion in the coatings, and the amount of permeable water per unit of time also decreased [43]. When the MrGO content was 3 wt.%, the surface of the coatings was relatively flat, and a small amount of blisters occurred. When the experiment was carried out for 240 h, cracks appeared on the surfaces of EP-rGO$_{0.5\%}$, EP-rGO$_{1\%}$, EP-rGO$_{2\%}$ and EP-rGO$_{4\%}$. While cracks were not present on the surface of EP-rGO$_{3\%}$, a large area of blistering was found.

In summary, when the MrGO content in the coatings was small, an effective barrier was not formed against the penetration of corrosive media. As the MrGO content increased, the penetration of corrosive media could be prevented. Furthermore, the agglomeration phenomenon increased to reduce the system capacity as the MrGO content gradually increased; as a result, the corrosion resistance of the MrGO/epoxy coatings decreased. MrGO/epoxy coatings are known to limit corrosion resistance; however, MrGO/epoxy coatings with 3 wt.% MrGO have the best corrosion resistance compared to other coatings.

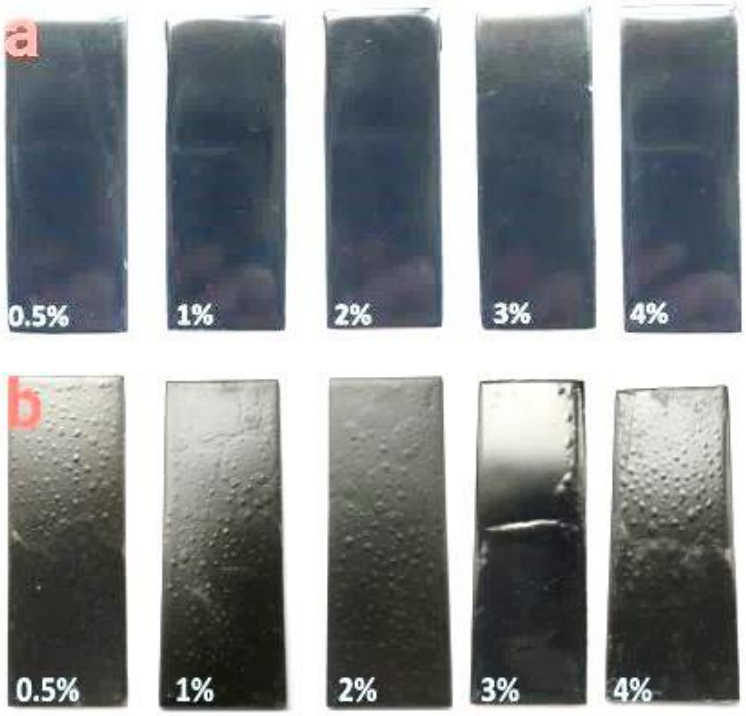

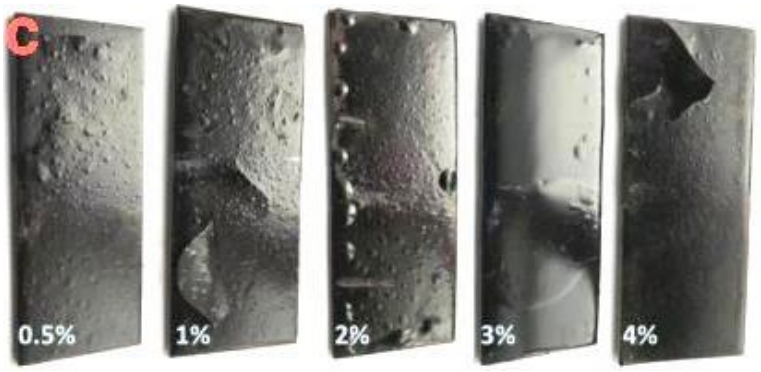

Figure 12. Morphology of the MrGO/epoxy coatings before and after high temperature and pressure immersion: (a) before immersion, (b) after soaking for 120 h, and (c) after soaking for 240 h.

3.8 Corrosion resistance processes

Fig. 13 shows a schematic diagram of the evolution of the corrosion resistance process for the MrGO/epoxy coatings with different MrGO contents. When epoxy resin and the curing agent were cured through a cross-linking reaction, a certain number of pores were formed in the epoxy coatings, through which corrosive media would permeate into the epoxy coatings, and the water contact angle was only 69.4° ± 1°.

rGO can be modified to maintain good dispersion and significantly optimize the bonding and compatibility with the epoxy coatings over a long period. The MrGO/epoxy coatings have good hydrophobicity, which reduces the contact area between the corrosive medium and the surface of the MrGO/epoxy coatings and reduces the amount of corrosive medium that can penetrate the MrGO/epoxy coatings.

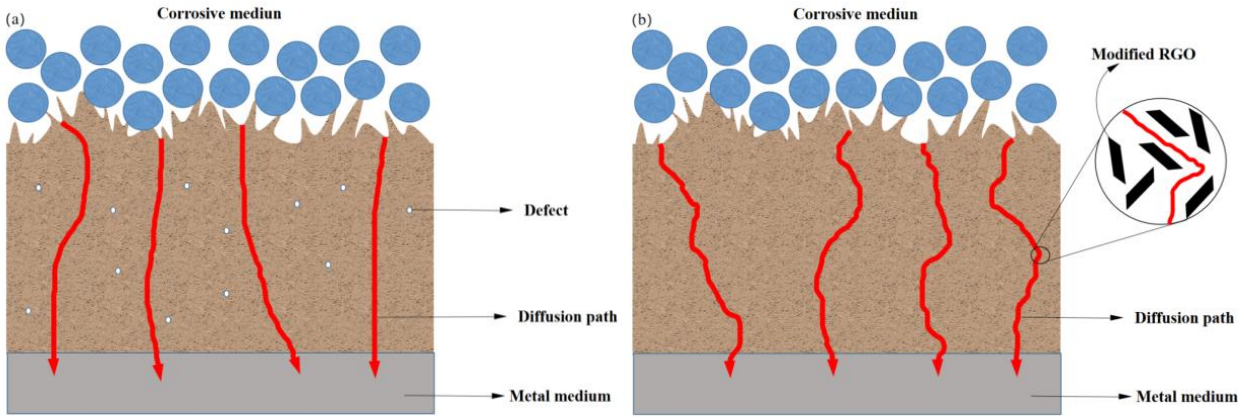

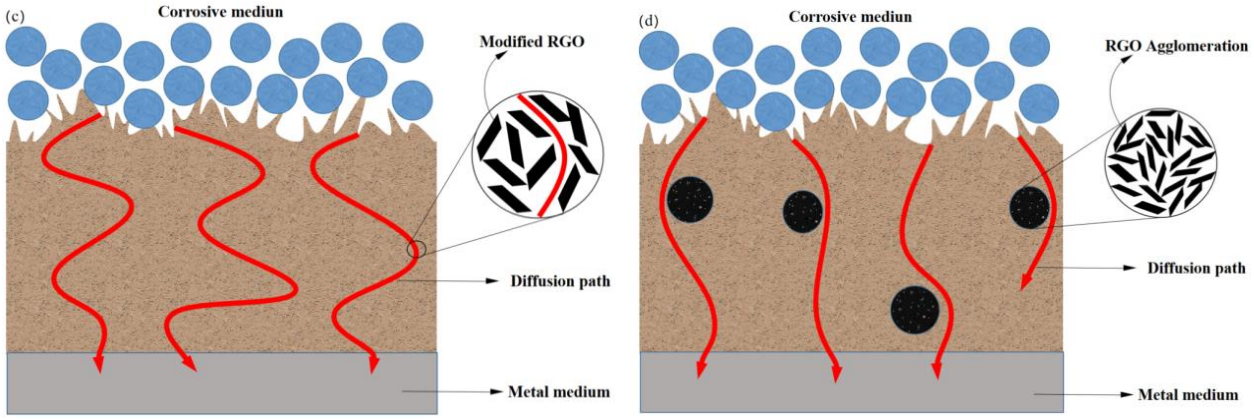

Figure 13. Schematic diagram of the evolution of the corrosion resistance of the coatings with different MrGO contents: (a) 0 wt.%, (b) 2 wt.%, (c) 3 wt.%, and (d) 4 wt.%

The water contact angle increased to 93.1° ± 1°, and the adhesion also increased when the MrGO content in the MrGO/epoxy coatings was 3 wt.%. However, 4 wt.% MrGO was added, the zeta potential of the coatings reached -29.5 mV. Combined with Fig. 5(f2), the red "island" area was fully covered, MrGO appeared agglomerated and overlapped, resulting in a decrease in its ionized H^+ amount, and the accumulation of defects in the form of hard particle volume increased. An increase in hard particles led to a reverse reduction in the dispersibility of MrGO. Then, the diffusion path for the corrosive medium in the MrGO/epoxy coatings increased.

Before the immersion tests, the adhesion of the epoxy coatings with and without MrGO did not change significantly. During immersion, the properties of the coatings all decreased, but the MrGO/epoxy coatings had better adhesion than the epoxy coatings. For the epoxy coatings, the corrosion medium was more likely to reach the interface between the coatings and the metal substrate and corrode the metal substrate. Corrosion products continued to accumulate at the interface, reducing the adhesion between the coatings and metal substrate, and then more metal substrate was exposed to the corrosive medium. Thus, a vicious cycle reducing the service time of the coatings was achieved. The addition of MrGO nanostructures to the epoxy coating could prolong the failure time of the coatings due to the "labyrinth effect" [44]. As shown in Fig. 13, the diffusion paths of the corrosive media in the epoxy coatings, EP-$MrGO_{2\%}$ and EP-$MrGO_{3\%}$, were gradually complicated. The excellent compatibility of MrGO with epoxy resin could reduce the probability of MrGO accumulation in the coatings, so the MrGO/epoxy coatings still showed single capacitance arc resistance after immersion for 120 h.

When the MrGO content was not sufficient, the composite coatings did not effectively block the penetration of the corrosive medium, and a double capacitance anti-arc was observed in the Nyquist impedance curve. With increasing MrGO content, E_{corr} gradually positively shifted, i_{corr} gradually decreased, and R_P gradually increased. However, an effective shield against corrosive media did not form until the MrGO content in the MrGo/epoxy coatings was 3 wt.%. At this time, a good dispersion of MrGO in the coating was achieved, the good filling of the pores could effectively block the diffusion of corrosive media, and then the diffusion path of corrosive media in the coatings was extended [45].

However, the diffusion paths began to simplify when the MrGO content reached 4 wt.%, because MrGO was prone to aggregation, and the interaction of the MrGO and the epoxy resin weakened, destroying the epoxy crosslinking network and reducing the thermal stability of the coatings. The voids between the agglomerates would become a favourite place for tiny bubbles to gather. When the MrGO/epoxy coatings were cured, pore defects and hard particles were formed in the coatings, and the MrGO/epoxy coating became brittle, causing failure of the MrGO/epoxy coatings as corrosion products were continuously produced and accumulated in the interface between the coatings and metal substrate.

4. CONCLUSIONS

(1) The MrGO content has a significant effect on the corrosion resistance of the coatings. When the MrGO content was less than 3 wt.%, an effective shield against the corrosive medium did not form. When the MrGO content was more than 3 wt.%, the MrGO agglomerated in the coatings, and the corrosion resistance of the coatings was also not strong. The MrGO/epoxy coatings with 3 wt.% MrGO had the best defensive performance.

(2) The addition of the MrGO enhanced the hydrophobicity, adhesion, and thermal stability properties of the coatings, and compared to the epoxy coatings, the corrosion resistance, wet adhesion, bonding, thermal stability, and corrosion resistance of EP-r$GO_{3\%}$ increased by 45.6%, 43%, 22.9%, and 2 orders of magnitude, respectively.

(3) The improvement in corrosion resistance of the coating is achieved in two ways: first, the staggered arrangement of the MrGO inside the coating provides a shield against the diffusion of corrosive media into the epoxy coating. It fills the internal pores and defects of the coating. Second, the MrGO gives the epoxy coating good hydrophobicity and reduces the contact area between the corrosive medium and the epoxy coating surface to reduce the corrosive medium's penetration into the epoxy coating.

ACKNOWLEDGEMENTS
This work was supported by the National Natural Science Foundation of China (51974245, 21808182), Key Research and Development Program of Shaanxi (2022GY-128, 2022SF-045), Scientific Research Program of Shaanxi Provincial Education Department (18JS088), Xi'an Science and Technology Planning Project (2020KJRC0097, 2020KJRC0098), Open Foundation of Shaanxi Key Laboratory of Carbon Dioxide Sequestration and Enhanced Oil Recovery, Postgraduate Innovation and Practical Ability Training Program (YCS21112076), and Youth Innovation Team of Shaanxi University.

References

1. L.T. Popoola, A.S. Grema, G.K. Latinwo, and B. Gutti, *Int. J. Ind. Chem.*, 4 (2013) 35.
2. M. Askari, M. Aliofkhazraei, and S. Afroukhteh, *J. Natural Gas Sci. Eng*., 71 (2019) 102971.
3. M Orazem, Underground pipeline corrosion: detection, analysis and prevention. Amsterdam: Elsevier, 2014.
4. J.L. Dawson, G. John, and K. Oliver, *Shreir's Corros.*, 4 (2010) 3230-3269.
5. L.T. Popoola, and A.S. Grema. Corrosion detection during oil and gas production and its

mitigation. LAP LAMBERT Academic Publishing, (2013) Saarbrücken, Germany.
6. K. Rajitha, and K. Mohana, *Diamond Relat. Mater.*, 108 (2020) 107974.
7. J. Wei, T. Vo, F. Inam, *RSC Adv.*, 5 (2015) 73510-73524.
8. D. Ratna. *J. Adhes. Sci. Technol.*, 17 (2003) 1655-1668.
9. J.H. Hodgkin, G.P. Simon, R.J. Varley. *Polym. Adv. Technol.*, 9 (2015) 3-10.
10. M.G. Hosseini, and K. Aboutalebi, *Prog. Org. Coat.*, 2018, 122 (2018) 56-63.
11. S.S. Golru, M.M. Attar, and B. Ramezanzadeh, *Prog. Org. Coat.*, 77 (2014) 1391-1399.
12. G. Christopher, M. Anbu Kulandainathan, and G. Harichandran, *Prog. Org. Coat.*, 89 (2015) 199-211.
13. P.A. Okafor, J. Singh-Beemat, and J.O. Iroh, *Prog. Org. Coat.*, 88 (2015) 237-244.
14. N. Jadhav, T. Matsuda, and V. Gelling, *J. Coat. Technol. Research*., 15 (2018) 363-374.
15. J. Chen, K. Kang, Y.W. Song, E.H. Han, S.D. Ma, and J.Q. Ao, *Coatings*, 9 (2019) 113.
16. T. Wang, H.Y. Ge, and K.L. Zhang, *J. Alloys Compd.*, 745 (2018) 705-715.
17. Y.C. Yang, Z.H. Xu, Z.W. Pan, and X.D. Li, *Adv. Mater.,* 24 (2012) 881-885.
18. S. Pourhashem, M.R. Vaezi, A. Rashidi, and M.R. Begherzadeh, *Corros. Sci.*, 115 (2016) 78-92.
19. K.C. Chang, M.H. Hsu, H.L. Liu, M.C. Lai, P.J. Liu, C.H. Hsu, W.F. Ji, T.L.Chuang, Y. Wei, J.M. Yeh, and W.R. Liu, *Carbon*, 66 (2014) 144-1531.
20. L. Al-Mashat, K. Shin, K. Kalantar-Zadeh, J.D. Plessis, S.H. Han, R.W. Kojima, R.B. Kaner, D. Li, X.L. Gou, S.J. Ippolito, and W. Wlodarski, *J. Phys. Chem. C,* 114 (2010) 16168-16173.
21. J.H. Ding, H.R. Zhao, B.Y. Xu, X.P. Zhao, S.P. Su, and H.B. Yu, *ACS Sustainable Chem. Eng.,* , 7 (2019) 10900-10911.
22. L. Gu, J.H. Ding, and H.B. Yu, *Prog. Chem.*, 28 (2016) 737-743.
23. K. Zhang, and S. Sharma, *ACS Sustainable Chem. Eng.*, 5 (2016) 277-286.
24. S.F. Hou, S.J. Su, M.L. Kasner, P. Shah, K. Patel, and C.J. Madarang, *Chem. Phys. Lett.*, 501 (2010) 68-74.
25. D. Zhang, Z.Y. Zhang, Y.Y. Liu, M.Q. Chu, C.Y. Yang, W.H. Li, Y.X. Shao, Y. Yue, and R.J. Xu. *Biomaterials*, 68 (2015) 100-113.
26. G. Gollavelli, and Y.C. Ling, *Biomaterials*, 33 (2012) 2532-2545.
27. A.N. Ganesh, E.N. Donders, B.K. Shoichet, and M.S. Shoichet, *Nano Today*, 19 (2018) 188-200.
28. V. Dahirel, and M. Jardat, *Curr. Opin. Colloid Interface Sci.*, 15 (2010) 2-7.
29. H.A. Becerril, J. Mao, Z.F. Liu, R.M. Stoltenberg, Z.N. Bao, and Y.S. Chen, *ACS Nano*, 2 (2008) 463-470.
30. J.F. Zhang, K. Kai, J. Yan, T. Wei, L.J. Zhi, J. Feng, Y.M. Ren, L.P. Song, and F. Wei, *ACS Nano*, 5 (2011) 191-198.
31. S.P. Vinodhini, and J.R. Xavier, *J. Mater. Sci.*, 56 (2021) 7094-7110.
32. J. Ding, Y. Huang, X. Sun, H.W. Wu, and Y.L. Wang, *J. Mater. Sci.: Mater. Electron.*, 27 (2016) 3462-3473.
33. H.W. Tien, Y.L. Huang, S.Y. Yang, S.T. Hsiao, W.H. Liao, H.M. Li, Y.S. Wang, J.Y. Wang, and C.C.M. Ma, *J Mater. Chem.*, 22 (2012) 2545-2552.
34. Y. Dong, Q.T. Lu, and Q.S. Yao, *Baosteel Tech. Res.*, 10 (2016) 15-20.
35. V.F. Lvovich, Impedance Spectroscopy: Applications to Electrochemical and Dielectric Phenomena. Wiley, (2012) Hoboken, America.
36. R.R. Nair, H.A. Wu, P.N. Jayaram, I.V. Grigorieva, and A.K. Geim, *Science*, 335 (2012) 442-444.
37. L.J. Zhu, C. Feng, and Y.Q. Cao, *Appl. Surf. Sci.*, 493 (2019) 889-896.
38. F. Bigdeli, M. Javidi, M. Pakshir, A. Khezrloo, and M. Tayebi, *Int. J. Pressure Vessels Pipin.*, 193 (2021) 104470.
39. F.A. Ghauri, M.A. Raza, M.S. Baig, and S. Ibrhim, *Mater. Res. Express*, 4 (2017) 125601.
40. Y. Hayatgheib, B. Ramezanzadeh, P. Kardar, and M. Mahdavian, *Corros. Sci.*, 133 (2018) 358-373.
41. N. Yang, T. Yang, W. Wang, H.Y. Chen, and W.H. Li, *J. Hazard. Mater.*, 377 (2019) 142-151.

42. L. Chen, L. Hui, Z.Q. Liu, and Q.H. Song, *Composites Part C: Open Access*, 5 (2021) 100124.
43. M. Jo, H.C. Lee, S.G. Lee, and K. Cho, *Carbon*, 116 (2017) 232-239.
44. S.X. Zhao, B.J. Dou, S. Duan, X.Z. Lin, and Y.J. Zhang, *RSC Adv*, 11 (2021) 17558-17573.
45. Y.M. Wu, F.W. Jiang, Y.J. Qiang, and W.J. Zhao, *Carbon*, 176 (2021) 39-51.